GANIT: Journal of Bangladesh Mathematical Society

GANIT*J. Bangladesh Math. Soc.* 46.3 (2026) 001–014
DOI: https://doi.org/10.3329/ganit.v46i01.89268

GANIT

Analysis of Casson Fluid Flow Past a Stretching Sheet Under Periodic Magnetic Field with Thermal Radiation and Chemical Reactions

Md. Yousuf Hossain[a*], Israt Jahan Luna[a], Tazrian Tamim[a], Jeba Tasnia[a], Salmoon Shefath[a], Sarder Firoz Ahmmed[a*]

[a]Mathematics Discipline, Khulna University, Khulna-9208, Bangladesh

ABSTRACT

This investigation explores the behavior of the unsteady non-Newtonian fluid (particularly Casson fluid) past a stretching sheet under the periodic magnetic field. Thermal radiation and higher order chemical reaction are also consider here. The governing equations for continuity, momentum, energy and concentration equation are formed by considering the aforementioned properties. In this study the time dependent governing equations are transformed properly into its non-dimensional form with the help of some dimensionless variables and quantities. A number of dimensionless parameters are obtained when the governing equations are nondimensionalized such as Grashof number (Gr), modified Grashof number (Gm), magnetic parameter (M), Prandtl number (Pr), radiation parameter (R), Dufour number (Du), Schimdt number (Sc), Soret number (Sr) and chemical reaction parameter (Kr). In order to getting the numerical solutions, the explicit finite difference method (EFDM) is used. This investigation provides the interaction of the non-dimensional parameters with some fluid properties like as velocity, temperature, concentration, skin friction, Nusselt number and Sherwood number. The application of non-Newtonian (Casson) fluid can be observed in many kinds of field like manufacturing industries, ink industries, polymer industries, food processing, medicine sectors and engineering sectors. The convergence analysis, along with the stabilization of numerical method has been established and it becomes conclude that the current study has conversed for $\mathrm{Pr} \geq 0.2422$ and $\mathrm{Sc} \geq 0.069$. The outcome of this research reveals that the movement of fluid can be dynamically influenced by fluctuations in non-dimensional parameters. Notably, the velocity profile is reduced with the increase of the Prandtl number and magnetic parameter.

Received: November 09, 2025 **Accepted:** April 27, 2026 **Published Online:** June 15, 2026
Keywords: Casson fluid; thermal radiation; periodic magnetic field; chemical reaction.

*Corresponding Author. *Email Address:* sfahmmed@math.ku.ac.bd, 211236yousuf@gmail.com

1. Introduction

The Casson fluid model was invented by the British mathematician and rheologist N. Casson in 1959. It is a one kind of fluid that cannot flow until a certain amount force is applied on it. Some researchers examined both analytical and numerical solutions for viscous fluid flow influenced by thermal radiation and chemical reactions past a vertical surface. Extensive research has been found out on fluid motion through porous

media, especially when considering the combined effects of thermal radiation, chemical reactions, and magnetic fields which showing their significant roles in industrial and mechanical engineering processes.
The behaviour of viscous fluid flow related to thermal radiation and chemical reactions can also be analysed for an infinite vertical permeable plate. In such cases, various parameters within the porous medium are taken into account, which govern the velocity, temperature, and concentration of the flow [1]. In recent years, many researchers have shown increasing interest in studying the boundary layer flow of Casson fluids over stretching porous surfaces subjected to thermal radiation. In such analyses, the governing equations were typically transformed into ordinary differential equations, which are then solved numerically [2].
Some two-dimensional Casson fluid flow model can also be solve by shooting method where partial differential equations are converted into ordinary differential equation by similarity transformations [3]. They considered surface temperature over an unsteady stretching surface. Their study revealed that variations in the unsteadiness parameter and the Prandtl number significantly influence the fluid velocity and temperature distribution.
K. K. Asogwa et al. [4] examined the magnetohydrodynamic (MHD) Casson fluid flow over a permeable stretching sheet, considering the effects of thermal radiation, heat, and mass transfer under various governing parameters. Their study highlighted the relevance of such flows in fields like astrophysics and geophysics.
J. K. Kigio et al. investigated the natural convective magnetohydrodynamic (MHD) flow of a copper engine oil nanofluid over a convectively heated vertical plate. A copper engine oil nanofluid is a suspension of copper nanoparticles dispersed in engine oil, resulting in improved thermal conductivity and heat transfer performance [5].
The comparative behaviour of Maxwell and Casson fluids was investigated by many researchers. The study revealed that parameters such as thermophoresis and radiation significantly contribute to enhancing the thermal boundary layer thickness. Moreover, an increase in the porous parameter was found to raise the heat transfer coefficient for the Casson fluid [6]. Several studies concluded that second-grade fluids exhibited higher velocity profiles and enhanced heat transfer compared to Newtonian fluids, although they demonstrated lower mass transfer rates. Such fluid flow behaviour has practical applications in various fields, including biomedical engineering, drug delivery systems, and food processing industries [7].
Reza-E-Rabbi et al. examined how nonlinear thermal radiation, a sinusoidal magnetic force, and Arrhenius activation energy influence the flow of a second-grade nanofluid over a porous stretching sheet [8]. Their findings revealed that nonlinear radiation notably raises the fluid temperature distribution, which is important for applications such as medical devices and ink manufacturing.
The study of hydrodynamic nanofluid flow over a nonlinearly stretching sheet under the influence of Hall current and thermal radiation highlighted that the combined effects of these factors play a crucial role in enhancing heat transfer characteristics [9]. The findings are particularly relevant to practical applications such as solar energy systems, nanoparticle-based cancer therapy, and polymer manufacturing processes.
Maxwell and Casson types of non-Newtonian fluids exhibit a stronger response compared to Newtonian fluids, resulting in more significant variations in temperature and velocity profiles [10, 11, 12].
The study on Williamson nanofluid flow over a porous stretching sheet subjected to a sinusoidal magnetic field revealed that the fluid exhibits higher velocity and temperature profiles compared to Newtonian fluids [13].
A time-dependent mixed convection flow with heat transfer was numerically investigated using nonlinear dimensionless governing PDEs with suitable boundary conditions [14]. The model was solved by the explicit finite difference method and the effects of the controlling physical parameters on velocity and temperature fields were examined through graphical results [14]. In this study some time dependent governing equations have been created and after making them non-dimensional explicit finite difference method (EFDM) was used to solve them. After solving them the interaction between some fluid properties like velocity profile, temperature profile, concentration profile, skin friction, rate of heat transfer and rate of mass transfer are showed in this study. This study explores the flow of a non-Newtonian (Casson) fluid over a stretched surface with the effects of a periodic magnetic field on the fluid's behaviour. The impact of thermal radiation and

chemical reaction of non-linear order are also considered.

Nomenclature

Variables	Interpretations	Parameters	Interpretations
x	Cartesian x coordinate	R	Radiation parameter
y	Cartesian y coordinate	Du	Dufour number
u	Velocity component in x direction	Sc	Schimdt number
v	Velocity component in y direction	Sr	Soret number
X	Non dimensional X coordinate	D_M	Chemical molecular diffusivity
Y	Non dimensional Y coordinate	Kr	Chemical reaction parameter
U	Dimensionless velocity component	K_T	Thermal diffusion ratio.
V	Dimensionless velocity component	T_M	Mean fluid temperature
g	Acceleration due to gravity	M	Magnetic parameter
t	Dimensional time	Gr	Grashof number
p	Reaction order	Gm	Mass Grashof number
q_r	Radioactive heat flux	Pr	Prandtl number
c_s	Concentration susceptibility	Greek Symbols	
c_p	Specific heat at constant pressure	U	Kinematic viscosity
T	Dimensional fluid temperature	λ	Wavelength
T_w	Fluid temperature at the wall	ρ	Density of the fluid
T_∞	Fluid temperature of uniform flow	σ	Electrical conductivity
C	Dimensional fluid concentration	β_T	Volumetric coefficient of thermal expansion
C_w	Fluid concentration at the wall	β_c	Volumetric coefficient of concentration expansion
C_∞	Fluid concentration outside the periphery	γ	Casson fluid parameter
k^*	Mean absorption co efficient	θ	Dimensionless fluid temperature
K_1	Chemical reaction rate	ϕ	Dimensionless fluid concentration
B_0	Magnetic field strength	κ	Thermal conductivity
D	Stretching constant	σ'	Boltzmann constant
		τ	Dimensionless time

2. Governing Equations

The rheological equation of state for an isotropic and incompressible flow of a Casson fluid is as follows,

$$\tau_{i,j} = \begin{cases} \left(\mu_B + \frac{p_y}{\sqrt{2\pi}}\right) 2e_{ij} & \pi > \pi_c \\ \left(\mu_B + \frac{p_y}{\sqrt{2\pi}}\right) 2e_{ij} & \pi < \pi_c \end{cases}$$

$\tau_{i,j}$ =Shear stress component
μ_B =Plastic dynamic viscosity
p_y =Yeild stress of the fluid
e_{ij} = Rate of deformation tensor
π = Second invariant of the stream rate tensor
π_c = Critical values of π

Thus the basic equations of unsteady two-dimensional free convective boundary layer flow of a viscous incompressible and electrically conducting fluid with constant viscosity and also constant thermal

conductivity past a vertical stretching plate in the presence of periodic magnetic field takes the following form continuity, momentum, energy, concentration equation and boundary condition which are (2.1), (2.2), (2.3), (2.4) and (2.5) respectively

$$\frac{\partial u}{\partial x}+\frac{\partial v}{\partial y}=0 \tag{2.1}$$

$$\frac{\partial u}{\partial t}+u\frac{\partial u}{\partial x}+v\frac{\partial u}{\partial y}=\upsilon\left(1+\frac{1}{\gamma}\right)\frac{\partial^2 u}{\partial y^2}+g\beta_T(T-T_\infty)+g\beta_c(C-C_\infty)-\frac{\sigma B_0^2}{\rho}\sin^2\left(\frac{\pi x}{\lambda}\right)u \tag{2.2}$$

$$\frac{\partial T}{\partial t}+u\frac{\partial T}{\partial x}+v\frac{\partial T}{\partial y}=\frac{\kappa}{\rho c_p}\frac{\partial^2 T}{\partial y^2}-\frac{1}{\rho c_p}\frac{\partial q_r}{\partial y}+\frac{D_M K_T}{c_s c_p}\frac{\partial^2 C}{\partial y^2} \tag{2.3}$$

$$\frac{\partial C}{\partial t}+u\frac{\partial C}{\partial x}+v\frac{\partial C}{\partial y}=D_M\frac{\partial^2 C}{\partial y^2}+\frac{D_M K_T}{T_M}\frac{\partial^2 T}{\partial y^2}-K_1(C-C_\infty)^p \tag{2.4}$$

$$u=Dx, v=0, T=T_w, C=C_w \text{ at } y=0$$
$$u=0, v=0, T\to T_\infty, C\to C_\infty \text{ as } y\to\infty \tag{2.5}$$

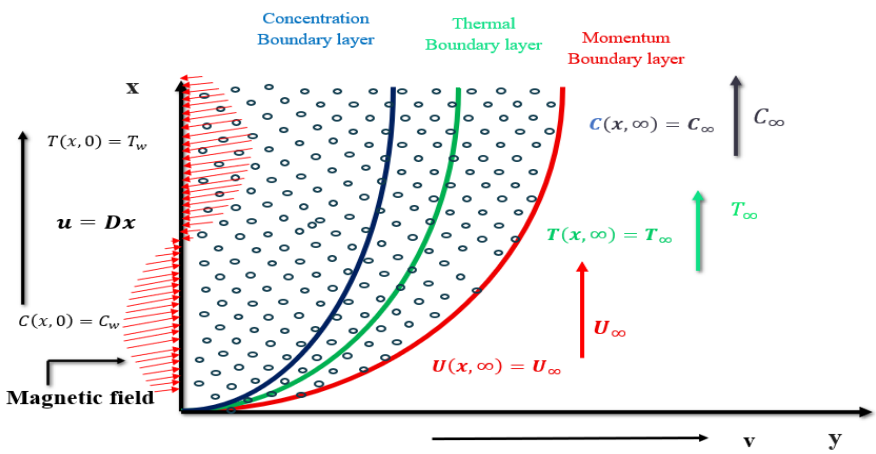

Fig. 2.1. Geometrical represent of fluid flow

The Rosseland approximation is in the form $q_r=-\frac{4\sigma'\partial(T^4)}{3k^*\partial y}$ here k^* and σ' are mean absorption co efficient and Boltzmann constant. Considering a very small temperature difference in the flow and expressing T^4 in a Taylor series about T_∞. Neglecting the higher ranked term, the obtained expression is

$$T^4\approx T_\infty^4+4T_\infty^3T-4T_\infty^3T_\infty\approx 4T_\infty^3T-3T_\infty^4$$

Then the equation (2.3) becomes

$$\frac{\partial T}{\partial t}+u\frac{\partial T}{\partial x}+v\frac{\partial T}{\partial y}=\frac{k}{\rho C_p}\frac{\partial^2 T}{\partial y^2}+\frac{16\sigma' T_\infty^3}{3k^*\rho c_p}\frac{\partial^2 T}{\partial y^2}+\frac{D_M K_T}{c_s c_p}\frac{\partial^2 C}{\partial y^2} \tag{2.6}$$

To solve the present problem with finite difference method, the following dimensionless variables and parameters are used to make the non-dimensional form of the above nonlinear coupled partial differential equation (2.1) to (2.5)

$$u=\frac{\upsilon}{\lambda}Gr^{\frac{1}{2}}U, v=\frac{\upsilon}{\lambda}Gr^{\frac{1}{4}}V, Y=\frac{y}{\lambda}Gr^{\frac{1}{4}}, X=\frac{x}{\lambda}, \tau=\frac{\upsilon}{\lambda^2}Gr^{\frac{1}{2}}t, \theta=\frac{T-T_\infty}{T_w-T_\infty}, \phi=\frac{C-C_\infty}{C_w-C_\infty}$$

2.1 Dimensionless Governing Equations

Therefore, the dimensionless representations of the crucial equations are

$$\frac{\partial U}{\partial X}+\frac{\partial V}{\partial Y}=0 \tag{2.7}$$

$$\frac{\partial U}{\partial \tau}+U\frac{\partial U}{\partial X}+V\frac{\partial U}{\partial Y}=\left(1+\frac{1}{\gamma}\right)\frac{\partial^2 U}{\partial Y^2}+\theta+\frac{Gm}{Gr}\phi-M^2\sin^2(\pi X)U \tag{2.8}$$

$$\frac{\partial \theta}{\partial \tau}+U\frac{\partial \theta}{\partial X}+V\frac{\partial \theta}{\partial Y}=\frac{1}{Pr}(1+R)\frac{\partial^2 \theta}{\partial Y^2}+Du\frac{\partial^2 \phi}{\partial Y^2} \tag{2.9}$$

$$\frac{\partial \phi}{\partial \tau}+U\frac{\partial \phi}{\partial X}+V\frac{\partial \phi}{\partial Y}=\frac{1}{Sc}\frac{\partial^2 \phi}{\partial y^2}+Sr\frac{\partial^2 \theta}{\partial y^2}-Kr\phi^p \tag{2.10}$$

Boundary condition

$$U=DX=D, V=0, \theta=1, \phi=1 \; at \; Y=0$$
$$U=0, V=0, \theta\to 0, \phi\to 0 \; as \; Y\to\infty \tag{2.11}$$

where,

The thermal Grashof number is defined as $Gr=\frac{g\beta_T\lambda^3(T_w-T_\infty)}{\upsilon^2}$, modified Grashof number is defined as $Gm=\frac{g\beta_C\lambda^3(T_w-T_\infty)}{\upsilon^2}$, magnetic parameter is $M^2=\frac{\sigma B_0^2\lambda^2}{\rho\upsilon G_r^{\frac{1}{2}}}$, Prandtl number defined as $Pr=\frac{kinematic\ viscosity}{Thermal\ diffusivity}=\frac{\mu c_p}{\kappa}$, radiation parameter denoted as $R=\frac{16\sigma^* T_\infty^3}{3k^*\kappa}$, Dufor number defined as $Du=\frac{D_m K_T}{\upsilon C_s C_p}\frac{(C_w-C_\infty)}{(T_w-T_\infty)}$, Schimdt number can express as $Sc=\frac{\upsilon}{D_m}$, Soret number denoted as $Sr=\frac{D_m K_T}{\upsilon T_m}\frac{(T_w-T_\infty)}{(C_w-C_\infty)}$, Chemical reaction parameter defined as $Kr=\frac{K_1^2\lambda^2}{\upsilon G_r^{\frac{1}{2}}}$.

3. Numerical analysis

The methodology used to solve the dimensionless governing equations (2.8) to (2.11) is described in this section, together with the associated boundary conditions. Because these time-dependent partial differential equations (PDEs) are highly nonlinear, obtaining an analytical solution is very challenging. Therefore, the proposed model is solved numerically using the widely adopted explicit finite difference (EFD) method. Applying the (EFDM) with those equations are given below

$$\frac{U_{i,j}-U_{i-1,j}}{\Delta X}+\frac{V_{i,j}-V_{i,j-1}}{\Delta Y}=0 \tag{3.1}$$

$$U'_{i,j}=\left(\left(1+\frac{1}{\gamma}\right)\frac{U_{i,j+1}-2U_{i,j}+U_{i,j-1}}{(\Delta Y)^2}+\theta_{i,j}+\frac{G_m}{G_r}\phi_{i,j}-M^2\sin^2(\pi X)U_{i,j}-U_{i,j}\frac{U_{i,j}-U_{i-1,j}}{\Delta X}-V_{i,j}\frac{U_{i,j+1}-U_{i,j}}{\Delta Y}\right)\Delta\tau+U_{i,j} \tag{3.2}$$

$$\theta'_{i,j}=\left(\frac{1}{P_r}(1+R)\frac{\theta_{i,j+1}-2\theta_{i,j}+\theta_{i,j-1}}{(\Delta Y)^2}+Du\frac{\phi_{i,j+1}-2\phi_{i,j}+\phi_{i,j-1}}{(\Delta Y)^2}-U_{i,j}\frac{\theta_{i,j}-\theta_{i-1,j}}{\Delta X}-V_{i,j}\frac{\theta_{i,j+1}-\theta_{i,j}}{\Delta Y}\right)\Delta\tau+\theta_{i,j} \tag{3.3}$$

$$\phi'_{i,j}=\left(\frac{1}{S_c}\frac{\phi_{i,j+1}-2\phi_{i,j}+\phi_{i,j-1}}{(\Delta Y)^2}+S_r\frac{\theta_{i,j+1}-2\theta_{i,j}+\theta_{i,j-1}}{(\Delta Y)^2}-K_r\phi_{i,j}^p-U_{i,j}\frac{\phi_{i,j}-\phi_{i-1,j}}{\Delta X}-V_{i,j}\frac{\phi_{i,j+1}-\phi_{i,j}}{\Delta Y}\right)\Delta\tau+\phi_{i,j} \tag{3.4}$$

4. Stability and convergence test

Since an explicit finite difference method is used, it is necessary to carry out both stability and convergence analyses for the problem. The following discussion outlines the expected stability conditions of the scheme for a uniform mesh. The time step Δt is omitted because it does not explicitly appear in equation (3.1) At the initial time $\tau=0$, the basic Fourier components for U, θ, and ϕ are represented by $e^{i\alpha x}e^{i\beta y}$. Based on

these assumptions, the corresponding equations at time τ can be derived.

$$\left.\begin{array}{l} U: F(t)e^{i\alpha X}\, e^{i\beta Y} \\ \theta: G(t)e^{i\alpha X}\, e^{i\beta Y} \\ \phi: H(t)e^{i\alpha X}\, e^{i\beta Y} \end{array}\right\} \tag{4.1}$$

Again,

$$\left.\begin{array}{l} U': F'(t)e^{i\alpha X}\, e^{i\beta Y} \\ \theta': G'(t)e^{i\alpha X}\, e^{i\beta Y} \\ \phi': H'(t)e^{i\alpha X}\, e^{i\beta Y} \end{array}\right\} \tag{4.2}$$

Now, replacing the values in equation (3.2) to (3.4) with those from (4.1) and (4.2) and if we consider U and V to be constants, following expression for momentum, energy and concentration equations can be obtained.

Form the momentum equation we can generate the below equation

$$\Rightarrow F' = F\left[1 - \frac{U(1-e^{-i\alpha\Delta X})\Delta\gamma}{\Delta X} - V\,\frac{(e^{i\beta\Delta Y}-1)\Delta\gamma}{\Delta X} + \frac{2\left(1+\frac{1}{r}\right)(\cos\beta\Delta Y-1)\Delta\gamma}{(\Delta Y)^2} - M^2\sin^2(\pi x)\,\Delta\tau\right] + G\Delta\tau + \frac{G_m}{Gr}H\Delta\tau$$

$$\Rightarrow \mathrm{F}' = \mathrm{A_1F} + \mathrm{A_2G} + \mathrm{A_3H}$$

where,

$$A_1 = 1 - \frac{U(1-e^{-i\alpha\Delta X})\Delta\tau}{\Delta X} - V\,\frac{(e^{i\beta\Delta Y}-1)\Delta\tau}{\Delta X} + \frac{2\left(1+\frac{1}{r}\right)(\cos\beta\Delta Y-1)\Delta\tau}{(\Delta Y)^2} - M^2\sin^2(\pi x)\,\Delta\tau$$

$$A_2 = \Delta\tau$$

$$A_3 = \frac{G_m}{Gr}\,\Delta\tau$$

Agan in for the energy equation we can write the below equation

$$\Rightarrow G' = G\left[1 + \frac{2}{Pr}(1+R)\,\frac{(\cos\beta\Delta Y-1)\Delta\tau}{(\Delta Y)^2} - \frac{(1-e^{-i\alpha\Delta X})\Delta\tau}{\Delta X}\,U - \frac{(e^{i\alpha\Delta\beta}-1)\Delta\tau}{\Delta Y}\,V\right] + 2H.Du\,\frac{(\cos\beta\Delta Y-1)\Delta\tau}{(\Delta Y)^2}$$

$$G' = 0.F + A_4G + A_5H$$

$$A_4 = 1 + \frac{2}{Pr}(1+R)\,\frac{(\cos\beta\Delta Y-1)\Delta\tau}{(\Delta Y)^2} - \frac{(1-e^{-i\alpha\Delta X})\Delta\tau}{\Delta X}\,U - \frac{(e^{i\alpha\Delta\beta}-1)\Delta\tau}{\Delta Y}\,V$$

$$A_5 = \frac{2Du\,(\cos\beta\Delta Y - 1)\Delta\tau}{(\Delta Y)^2}$$

For the concentration equation the below equation can be made

$$\Rightarrow H' = H\left[1 - \frac{U(1-e^{-i\alpha\Delta X})\Delta\tau}{\Delta X} - V\,\frac{(e^{i\alpha\Delta\beta}-1)\Delta\tau}{\Delta Y} + \frac{2}{Sc}\,\frac{(e^{i\alpha\Delta\beta}-1)\Delta\tau}{(\Delta Y)^2} - Kr.\emptyset^{P-1}\,\Delta\tau\right] + 2Sr.G\,\frac{(\cos\beta\Delta Y-1)}{(\Delta Y)^2}$$

$$\Rightarrow H' = 0.F + A_6G + A_7H$$

$$A_7 = \left[1 - \frac{U(1-e^{-i\alpha\Delta X})\Delta\tau}{\Delta X} - V\,\frac{(e^{i\alpha\Delta\beta}-1)\Delta\tau}{\Delta Y} + \frac{2}{Sc}\,\frac{(e^{i\alpha\Delta\beta}-1)\Delta\tau}{(\Delta Y)^2} - Kr.\emptyset^{P-1}\,\Delta\tau\right]$$

$$A_6 = 2Sr\,\frac{(\cos\beta\Delta Y-1)\Delta\tau}{(\Delta Y)^2}$$

So, the generated equations are

$$F' = A_1{}^{+} + \mathrm{A_2G} + \mathrm{A_3H}$$

$$G' = 0.F + A_4G + A_5H$$

$$H' = 0.F + A_6G + A_7H$$

In the matrix from above equations looks like this

$$\begin{bmatrix} F' \\ G' \\ H' \end{bmatrix} = \begin{bmatrix} A_1 & A_2 & A_3 \\ 0 & A_4 & A_5 \\ 0 & A_6 & A_7 \end{bmatrix}\begin{bmatrix} F \\ G \\ H \end{bmatrix}$$

It can be represented as

$\eta' = T'\eta$

$\eta' = \begin{bmatrix} F' \\ G' \\ H' \end{bmatrix}, \quad T' = \begin{bmatrix} A_1 & A_2 & A_3 \\ 0 & A_4 & A_5 \\ 0 & A_6 & A_7 \end{bmatrix}, \eta = \begin{bmatrix} F \\ G \\ H \end{bmatrix}$

Studying at diverse values of T' is challenging. A small time step $\Delta\tau \to 0$ is taken into the account. So the following expression may be found for $A_2 \to 0, A_3 \to 0, A_4 \to 0$. Hence, $T' = \begin{bmatrix} A_1 & 0 & 0 \\ 0 & A_4 & 0 \\ 0 & 0 & A_7 \end{bmatrix}$

The eigenvalues of T' thus obtained as follows

$\lambda_1 = A_1, \lambda_2 = A_4, \ \lambda_3 = A_7$

The stability postulates is a follows

$|A_1| \leq 1, |A_4| \leq 1, |A_7| \leq 1$

again consider as

$a' = \Delta\tau, \ b' = U\frac{\Delta\tau}{\Delta X}, c' = |-\mathrm{V}|\frac{\Delta\tau}{\Delta X}, d' = \frac{2\Delta\tau}{(\Delta Y)^2}$

$A_1 = 1 - 2\left[b' + c' + \left(1 + \frac{1}{r}\right)d' + M^2\sin^2(\pi x)\frac{a'}{2}\right]$

$A_4 = 1 - 2\left[\frac{1}{Pr}(1+R)d' + b' + c'\right]$

$A_7 = 1 - 2\left[b' + c' + \frac{1}{Sc}\, d' - \ Kr.\phi^{P-1}\ \frac{a'}{2}\right]$

The maximum negative bounded values of A_1, A_4, A_7 are -1. so, stablity conditions are,

$$\left(1 + \frac{1}{r}\right)2\frac{\Delta\tau}{(\Delta Y)^2} + U\ \frac{\Delta\tau}{\Delta X} + V\frac{\Delta\tau}{\Delta Y} + M^2\sin^2(\pi x)\ \leq 1$$

$$\frac{2}{Pr}(1+R)\frac{\Delta\tau}{(\Delta Y)^2} + U\ \frac{\Delta\tau}{\Delta X} + V\frac{\Delta\tau}{\Delta Y} \leq 1$$

$$\frac{2}{Sc}\ \frac{\Delta\tau}{(\Delta Y)^2} + U\ \frac{\Delta\tau}{\Delta X} + V\frac{\Delta\tau}{\Delta Y} + \ Kr.\phi^{P-1}\ \frac{\Delta\tau}{2}\ \leq 1$$

Here the fundamental initially boundary conditions are given by, $U = 0, \theta = 0, \phi = 0, \ \Delta\tau = 0.001, \Delta X = 0.15, \ \Delta Y = 0.17$ Hence,

$$\left(1 + \frac{1}{r}\right)2\frac{\Delta\tau}{(\Delta Y)^2} + \frac{M^2\sin^2(\pi x)\,\Delta\tau}{2} \leq 1 \tag{4.3}$$

$$\frac{2}{Pr}(1+R)\frac{\Delta\tau}{(\Delta Y)^2} \leq 1 \tag{4.4}$$

$$\frac{2}{Sc}\ \frac{\Delta\tau}{(\Delta Y)^2} - Kr\ \frac{\Delta\tau}{2} \leq 1 \tag{4.5}$$

For equation (4.4) if we put radiation parameter R=2.5 then we can write

$$\frac{2}{Pr}(1+2.5)\ \frac{0.001}{(0.17)^2} \leq 1$$

$$So, Pr \geq 0.2422$$

Similarly, from (4.5) Kr=1.50 then Sc≥0.069

The convergence analysis, along with the stabilization of the numerical method is performed, showing that the governing equation converges for $Pr \geq 0.2422$ and Sc≥0.069

5. Graphical Analysis

The graphs are generated by using a few default parameters values such as M=1.0 γ=1.0, Gm=7.0, Gr=7.0, Pr =1.0, R= 2.5, Du =1.0, Sc=1.0, Sr=1.5 and Kr= 1.5

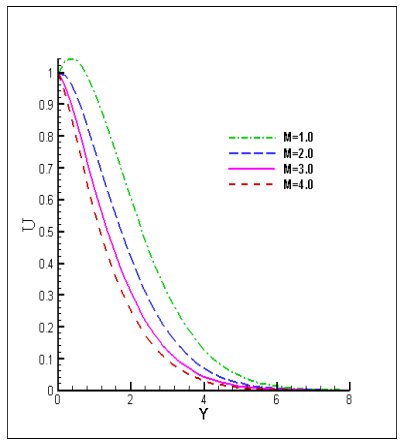

Fig. 5.1. Effects of magnetic parameter (M) on velocity profile.

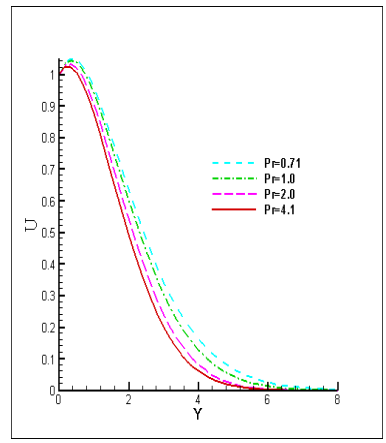

Fig. 5.2 Effects of Prandtl number (Pr) on velocity profile.

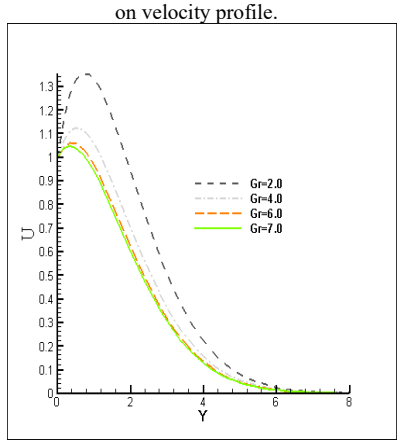

Fig. 5.3. Effects of Grashof number (Gr) on velocity profile.

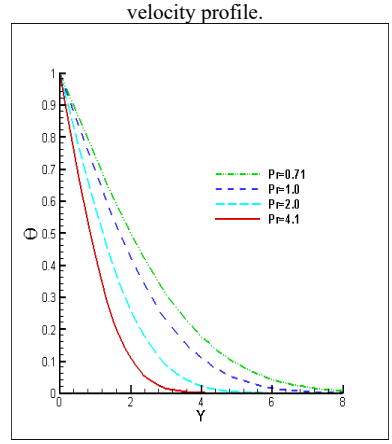

Fig. 5.4. Effects of Prandtl number (Pr) on temperature profile.

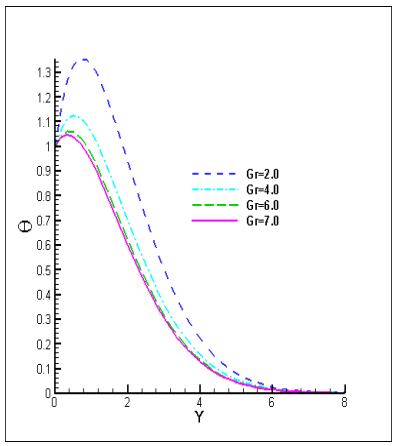

Fig. 5.5. Effects of Grashof number (Gr) on temperature profile.

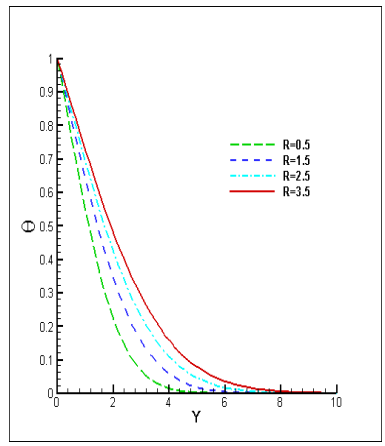

Fig. 5.6. Effects of radiation parameter (R) on temperature profile.

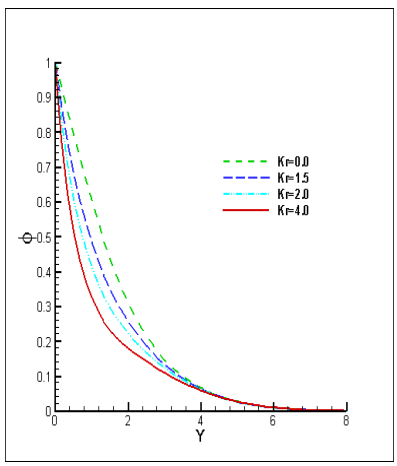

Fig. 5.7. Effects of chemical reaction parameter (Kr) on concentration profile.

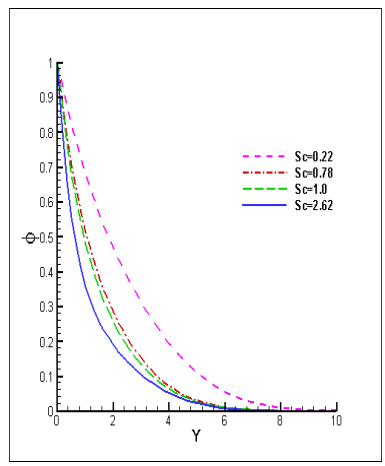

Fig. 5.8. Effects of Schimdt number (Sc) on concentration profile.

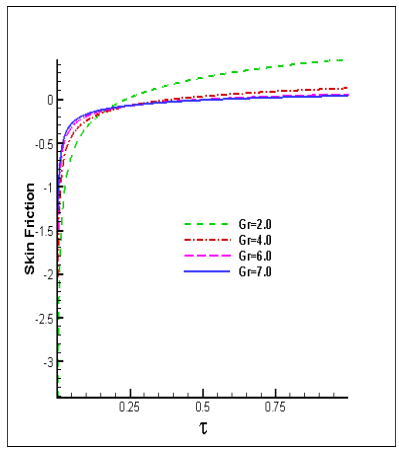

Fig. 5.9. Effects of Grashof number (Gr) on skin friction.

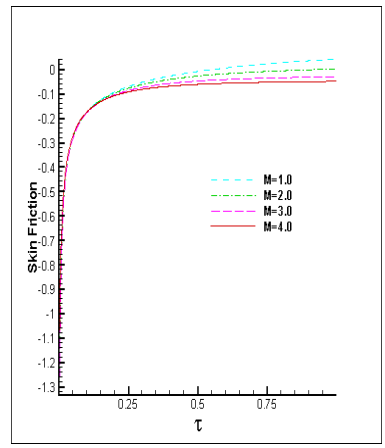

Fig. 5.10. Effects of magnetic parameter (M) on skin friction.

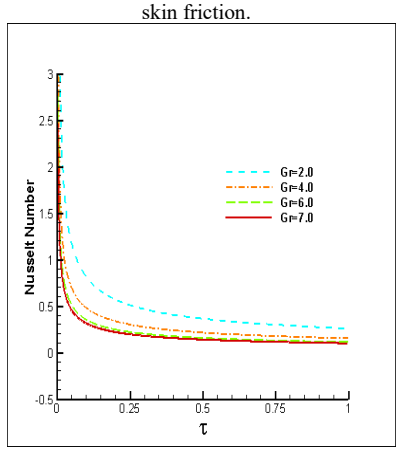

Fig. 5.11. Effects of Grashof number (Gr) on Nusselt number.

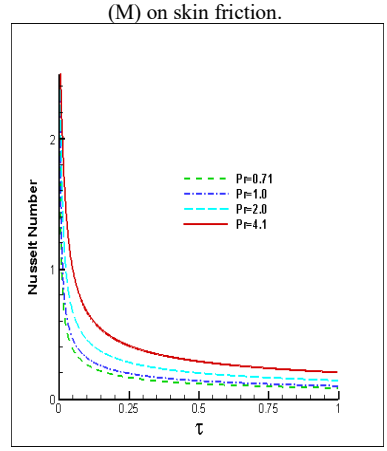

Fig. 5.12. Effects of Prandtl number (Pr) on Nusselt number.

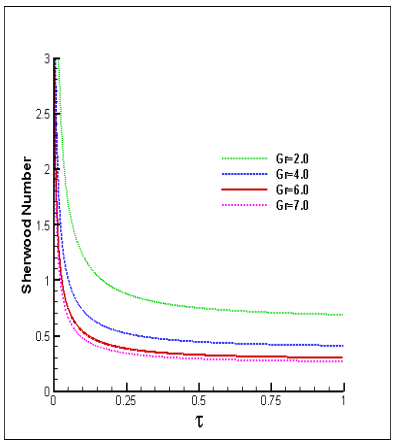

Fig. 5.13. Effects of Grashof number (Gr), on Sherwood number.

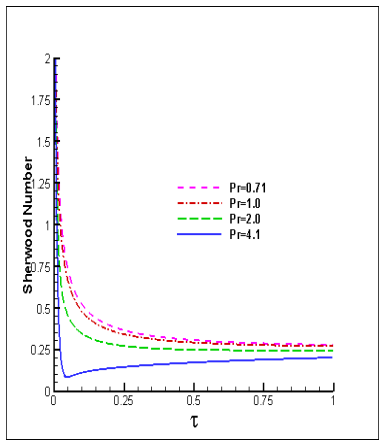

Fig. 5.14. Effects of Prandtl number (Pr) on Sherwood number.

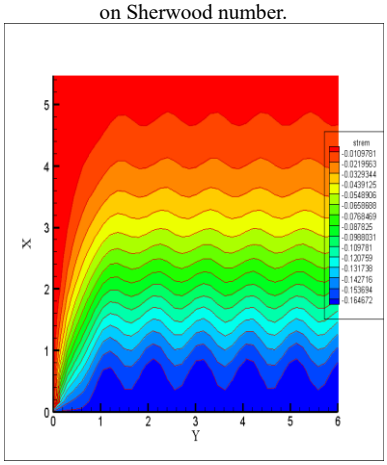

Fig. 5.15. Effects of Streamlines

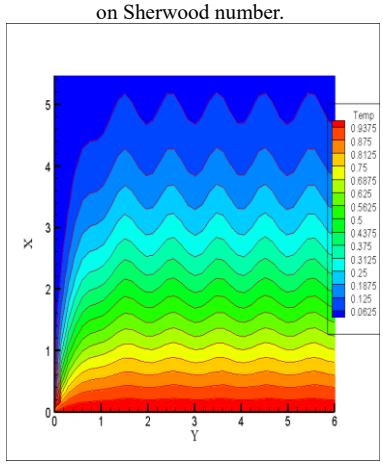

Fig. 5.16. Effects of Isothermal lines

6. Result and Discussion

In this section the movement of fluid (particularly Casson fluid) is inspected by different values of well known parameters. The movement properties of the Casson fluid include velocity profile, concentration profile, temperature profile, skin friction, Nusselt number, Sherwood number has been illustrated. For the effect of many parameters like Grashof number (Gr), modified Grashof number (Gm), magnetic parameter (M), radiation parameter (R), Prandtl number (Pr), Dufour number (Du), Soret number (Sr), Schimdt number (Sc) and chemical reaction parameter (Kr), the movement of the fluid can be bend.

6.1. Velocity

As the magnetic field impact increases periodically, the velocity profile oscillates Fig 5.1. and is measured along the Y-coordinate. Increasing the magnetic parameter (M) reduces the fluid velocity. For example, at Y = 2.00669, the velocity decreases from 0.59783 (M=1.0) to 0.41263 (M=2.0), 0.30428 (M=3.0), and 0.24631 (M=4.0). On average, the velocity drops by about 8.788% per unit increase in (M). Fig 5.2. shows that the velocity profile changes with the Prandtl number (Pr). The velocity slightly decreases as (Pr) increases. At Y = 0.33445, the maximum velocity drops from 1.05193 (Pr=0.71) to 1.04569 (Pr=1.0), 1.03351 (Pr=2.0), and 1.02269 (Pr=4.1). Similarly, at Y = 2.00669, the velocity decreases from 0.63072 to

0.59783, 0.53753, and 0.48808 for the same Pr values. Overall, the average velocity reduction is about 4.2% per unit increase in Pr. Fig 5.3. shows that the fluid velocity is influenced by the Grashof number (Gr). As Gr increases, the velocity profile gradually decreases. At Y = 2.00669, the Casson fluid velocity drops from 0.93570 (Gr=2.0) to 0.69844 (Gr=4.0), 0.62012 (Gr=6.0), and 0.59773 (Gr=7.0), indicating a clear reduction in velocity with higher Gr values. The maximum velocity values are 1.35609, 1.12526, 1.306037, and 1.04569 for Gr = 2.0, 4.0, 6.0, and 7.0, occurring at Y = 0.66890, 0.50167, 0.33445, and 0.33445, respectively.

6.2. Temperature

Fig 5.4. indicates the temperature distribution for different values of the Prandtl number. It shows that higher values of the Prandtl number (Pr) are responsible for diminishing the temperature profile. At the fixed position Y=2.00669, the temperature values are 0.49823, 0.42196, 0.25728, and 0.10633 for Pr=0.71, Pr=1.0, Pr=2.0, and Pr=4.1, respectively. Finally, the average rate of temperature reduction is 9.31% per unit increase in Pr. Fig 5.5. illustrates that the fluid temperature is also affected by different values of the Grashof number (Gr). Increasing values of Gr reduce the temperature profile. As the Grashof number increases, the temperature profile gradually decreases. Specifically, at Y=2.00669, the Casson fluid temperature is 0.42824, 0.42371, 0.42232, and 0.42196 for Gr=2.0, Gr=4.0, Gr=6.0, and Gr=7.0, respectively. This clearly indicates that rising values of Gr diminish the temperature profile. Fig 5.6. presents the temperature distribution for different values of the radiation parameter (R). The temperature varies significantly with increasing R. Higher values of the radiation parameter increase the fluid temperature. At Y=2.00669, the fluid temperatures are 0.22142, 0.34256, 0.42196, and 0.47851 for R=0.50, R=1.50, R=2.50, and R=3.50, respectively. Therefore, an increase in the radiation parameter leads to an increase in the fluid temperature.

6.3. Concentration

Fig 5.7. shows that increasing the chemical reaction parameter (Kr) steadily reduces the concentration profile. At Y = 2.00669, the concentration decreases from 0.30778 (Kr = 0.0) to 0.17951 (Kr = 4.0), with an average drop of 3.47% per unit rise in (Kr). Fig 5.8. confirms that the Schimdt number (Sc) also affects concentration. Higher Sc values lower the concentration, while lower Sc values increase it. At Y = 2.00669, the concentration falls from 0.46758 (Sc = 0.22) to 0.25573 (Sc = 1.0), showing an average reduction of 11.58% per unit increase in Schimdt number.

6.4. Skin Friction, Nusselt Number and Sherwood Number

Fig 5.9. and Fig 5.10. show the effect of skin friction, which increases when the values of the Grashof number and the magnetic parameter decrease. Lower values of the Grashof number are responsible for increasing the rate of heat transfer, as shown in Fig 5.11. In Fig 5.12. it can clearly be seen that higher values of the Prandtl number (Pr) increase the Nusselt number. The rate of mass transfer decreases when Gr and Pr are increased, as illustrated in Fig 5.13. and Fig 5.14. Streamline profiles are presented to provide a clearer visualization of the fluid flow field, representing the direction and behaviour of fluid velocity. The isotherms, on the other hand, depict variations within the boundary layer where the temperature remains constant.

6.5. Streamlines and isothermal lines

Fig 5.15. and Fig 5.16. present the graphical representations of both the streamline and isotherm patterns. These plots are generated for the parameter values Gr=7.0, γ=1.0, Gm=7.0, M=1.0, Pr=1.0, R=2.5, Du=1.0, Sc=1.0, Sr=1.5, and Kr=1.5.

7. Conclusions

In this paper we have studied the behaviour of the unsteady non-Newtonian fluid (particularly Casson fluid) past a stretching sheet under the periodic magnetic field. Non-Newtonian (Casson) fluid behaviour is commonly observed in many practical fields, for examples manufacturing process industries, ink industries, polymer industries, food processing, medicine sectors and engineering sectors. The key results of the current study can be outlined as below:

- An increase in the magnetic parameter (M), Prandtl number (Pr), and Grashof number (Gr) causes the velocity profile to decrease.

- Lower values of the Prandtl number (Pr) and Grashof number (Gr) lead to an increase in the temperature profile, whereas a decrease in the radiation parameter causes the temperature profile to decline.
- The concentration profile exhibits a decreasing trend with increasing values of the chemical reaction parameter (Kr) and Schimdt number (Sc).
- With increasing Grashof number (Gr) and magnetic parameter (M), the skin friction profile shows a decreasing trend
- The variation in Nusselt number indicates that it increases with the enhancement of the Prandtl number (Pr) and the reduction of the Grashof number (Gr).
- An inverse relationship exists between the Sherwood number and the increasing values of Grashof number (Gr) and Prandtl number (Pr).
-

Acknowledgements
The research by S.F. Ahmmed et al. was partially supported by Khulna University.

References

[1] Gharami, P. P., Arifuzzaman, S. M., Reza-E-Rabbi, S., Khan, M. S., & Ahmmed, S. F. (2020). Analytical and numerical solution of viscous fluid flow with the effects of thermal radiation and chemical reaction past a vertical porous surface. International Journal of Heat and Technology, 38(1), 689–700.
[2] Pramanik, S. (2013). Casson fluid flow and heat transfer past a stretching surface. Ain Shams Engineering Journal, 5(2), 205–212.
[3] Mukhopadhyay, S., De, P. R., Bhattacharyya, K., & Layek, G. (2013). Casson fluid flow over an unsteady stretching surface. Ain Shams Engineering Journal, 4(3), 933–938.
[4] Asogwa, K. K., & Ibe, A. A. (2020). A study of MHD Casson fluid flow over a permeable stretching sheet with heat and mass transfer. Journal of Engineering Research and Reports, 16(4), 10–25.
[5] Kigio, J. K., Nduku, M. W., & Samuel, O. A. (2021). Analysis of volume fraction and convective heat transfer on MHD Casson nanofluid over a vertical plate. Fluid Mechanics, 7(5), 1–8.
[6] Reza-E-Rabbi, S., Ahmmed, S. F., Arifuzzaman, S., Sarkar, T., & Shakhaoath, M. (2019). Computational modelling of multiphase fluid flow behaviour over a stretching sheet in the presence of nanoparticles. Engineering Science and Technology, 23(6), 605–617.
[7] Ahmmed, S. F., Ali, M. Y., & Reza-E-Rabbi, S. (2024). Comparative analysis with data prediction of nonlinear radiative nanofluid with magnetic force. Partial Differential Equations in Applied Mathematics, 11, 100760.
[8] Reza-E-Rabbi, S., Ali, M. Y., & Ahmmed, S. F. (2024). Nonlinear radiative second-grade nanofluid with sinusoidal magnetic force and Arrhenius activation energy: A computational exploration. Alexandria Engineering Journal, 104, 66–84.
[9] Ali, M. Y., Reza-E-Rabbi, S., Rasel, M. M. H., & Ahmmed, S. F. (2023). Combined impacts of thermoelectric and radiation on hydromagnetic nanofluid flow over a nonlinear stretching sheet. Partial Differential Equations in Applied Mathematics, 7, 100500.
[10] Ali, M. Y., Reza-E-Rabbi, S., Ahmmed, S. F., Nabi, M. N., Azad, A. K., & Muyeen, S. (2024). Hydromagnetic flow of Casson nanofluid across a stretched sheet in the presence of thermoelectric and radiation. International Journal of Thermofluids, 21, 100484.
[11] Reza-E-Rabbi, S., Arifuzzaman, S. M., Sarkar, T., Khan, M. S., & Ahmmed, S. F. (2019). Periodic magnetohydrodynamic simulation of Newtonian and non-Newtonian fluid flow past a stretching sheet with nanoparticles. AIP Conference Proceedings, 2121, 070006.
[12] Islam, S., Ali, M. Y., & Reza-E-Rabbi, S. (2024). Comparative simulation of nonlinear radiative nano Casson and Maxwell fluids with periodic magnetic force and sensitivity analysis. Heliyon, 10(12), e29306.
[13] Tamanna, T., & Ahmmed, S. F. (2025). Computational modeling of radiative Williamson nanofluid flow under periodic magnetic force. International Journal of Thermofluids, 26, 101065.

[14] Kamrujjaman, M. A. H., & Md. J. A. (2016). Mixed convection flow along a horizontal circular cylinder with small amplitude oscillation in surface temperature and free stream. Mechanical Engineering Research, 6(2), 34–47.